Remote Sensing of Environment 115 (2011) 586–599

Contents lists available at ScienceDirect

Remote Sensing of Environment

journal homepage: www.elsevier.com/locate/rse

Leaf area index estimation with MODIS reflectance time series and model inversion during full rotations of *Eucalyptus* plantations

Guerric le Maire [a,b,*], Claire Marsden [a], Wouter Verhoef [c], Flávio Jorge Ponzoni [d], Danny Lo Seen [b], Agnès Bégué [b], José-Luiz Stape [e], Yann Nouvellon [a,f]

[a] CIRAD, Persyst, UPR 80, s/c UMR Eco&Sols, 2 Place Viala - bât 12, 34060 Montpellier Cedex 01, France
[b] CIRAD, UMR TETIS, Maison de la Télédétection, 34093 Montpellier Cedex 5, France
[c] Faculty of Geo-Information Science and Earth Observation (ITC), University of Twente, Enschede, The Netherlands
[d] National Institute for Space Research (INPE), Remote Sensing Department, 12227-010 São José dos Campos, SP, Brazil
[e] Department of Forestry and Environmental Sciences, North Carolina State University, Raleigh, NC 27695, United States
[f] Departamento de Ciências Atmosféricas, IAG, Universidade de São Paulo, Brazil

ARTICLE INFO

Article history:
Received 20 April 2010
Received in revised form 23 September 2010
Accepted 12 October 2010

Keywords:
Leaf area index
Remote sensing
MOD13Q1
Radiative transfer model
PROSAIL
GESAVI
Eucalypt
CBERS

ABSTRACT

The leaf area index (LAI) of fast-growing *Eucalyptus* plantations is highly dynamic both seasonally and inter-annually, and is spatially variable depending on pedo-climatic conditions. LAI is very important in determining the carbon and water balance of a stand, but is difficult to measure during a complete stand rotation and at large scales. Remote-sensing methods allowing the retrieval of LAI time series with accuracy and precision are therefore necessary. Here, we tested two methods for LAI estimation from MODIS 250m resolution red and near-infrared (NIR) reflectance time series. The first method involved the inversion of a coupled model of leaf reflectance and transmittance (PROSPECT4), soil reflectance (SOILSPECT) and canopy radiative transfer (4SAIL2). Model parameters other than the LAI were either fixed to measured constant values, or allowed to vary seasonally and/or with stand age according to trends observed in field measurements. The LAI was assumed to vary throughout the rotation following a series of alternately increasing and decreasing sigmoid curves. The parameters of each sigmoid curve that allowed the best fit of simulated canopy reflectance to MODIS red and NIR reflectance data were obtained by minimization techniques. The second method was based on a linear relationship between the LAI and values of the GEneralized Soil Adjusted Vegetation Index (GESAVI), which was calibrated using destructive LAI measurements made at two seasons, on *Eucalyptus* stands of different ages and productivity levels. The ability of each approach to reproduce field-measured LAI values was assessed, and uncertainty on results and parameter sensitivities were examined. Both methods offered a good fit between measured and estimated LAI ($R^2 = 0.80$ and $R^2 = 0.62$ for model inversion and GESAVI-based methods, respectively), but the GESAVI-based method overestimated the LAI at young ages.

1. Introduction

Leaf area index (LAI) is a key parameter involved in a variety of ecosystem processes, such as light and rain interception, transpiration, photosynthesis, plant respiration, and soil heterotrophic respiration (through litter fall). Its precise temporal and spatial estimation is crucial for the understanding of forest processes and for the parameterization of ecosystem models that quantify carbon, water, and energy fluxes.

Field estimations of LAI are often performed using optical (LICOR LAI-2000, hemispherical photographs), direct and semi-direct methods (litter collection, allometric methods, and destructive sampling). Routine in-situ measurements of LAI are, however, time-consuming and even unfeasible for large scale studies. For this reason, numerous studies have attempted to characterize LAI with remotely sensed data (North, 2002; Rouse et al., 1973). The reflectance deduced from satellite measurements contains information on canopy structural and biochemical characteristics. In particular, reflectance in the visible and near-infrared wavelengths is highly sensitive to green LAI, thus offering the challenging opportunity of quantifying LAI using reflectance values. Two types of methods have classically been used for this purpose:

– *Spectral Vegetation Indices and/or multiple regressions*: mathematical combinations of well-chosen spectral band reflectances are designed to correlate with particular characteristics of the observed surface. These methods are simple, but their use is limited to the representativeness of the experimental calibration

* Corresponding author. CIRAD, Persyst, UPR 80, s/c UMR Eco&Sols, 2 Place Viala - bât 12, 34060 Montpellier Cedex 01, France. Tel.: +33 4 67 54 87 64; fax: +33 4 67 54 87 00.
E-mail address: guerric.le_maire@cirad.fr (G. le Maire).

0034-4257/$ – see front matter © 2010 Elsevier Inc. All rights reserved.
doi:10.1016/j.rse.2010.10.004

dataset. Moreover, indices and multiple regressions may be sensitive to more than a single characteristic. They are also more or less sensitive to vegetation type, atmospheric conditions, viewing geometry, spatial resolution, and therefore they must generally be calibrated for each image (Thenkabail et al., 2000; Turner et al., 1999; Walthall et al., 2004).

– *Inversion of Radiative Transfer Models (RTM)* that simulate reflectance spectra from canopy and soil characteristics. Existing RTM belong to a range of types (simple turbid-medium, geometrical models, hybrid models, and discrete or ray-tracing models), each offering a different representation of the spatial heterogeneity of a scene.

Inversion techniques are based on minimization algorithms, or on pre-computed reflectance databases using either Look-Up Tables (Knyazikhin et al., 1998) or Neural Networks (Bacour et al., 2006; Baret et al., 2007; Fang & Liang, 2005). The inversion of such reflectance models often gives a large number of different possible solutions and therefore needs to be constrained. Moreover, uncertainties on measurements and models may result in a large variability in the results (Combal et al., 2003).

These two methods have their advantages and drawbacks, and the choice of a method highly depends on the characteristics of the vegetation and on the objective of the study.

In this study, we focus on the particular case of *Eucalyptus* plantations. *Eucalyptus* trees, which are the most widely planted hardwood genus in tropical regions (FAO, 2006), provide an increasing share of the global wood supply. The fast-growing *Eucalyptus* plantations of São Paulo State (Brazil) have a rotation length of typically 5 to 7 years (Laclau et al., 2010). Large structural changes of the canopy occur during this time: the rapid growth from seedlings to high trees (up to >25 m) is accompanied by changes in LAI, crown cover, leaf angles, specific leaf area (SLA), etc. (Laclau et al., 2009, 2010; Marsden et al., 2010). Plantations also experience seasonal changes mainly because of the dry season when trees are water limited (Almeida et al., 2007). The LAI of *Eucalyptus* plantations largely determines plantation carbon and water cycles (du Toit, 2008; Marsden et al., 2010), and hence wood production and water consumption. The retrieval of LAI time series is therefore an important objective both for plantation managers (who are now increasingly using process-based models to monitor and predict production), and for scientists interested in biogeochemical modeling to address carbon sequestration, water use and sustainability issues. The methods currently available involve a great deal of field and interpretation work (regular visits of inventory plots with some optical device to measure gap fractions), and are therefore unsatisfactory regarding time- and cost-effectiveness, but also accuracy and spatial representation. LAI estimation using remote sensing is therefore highly relevant but also challenging for this ecosystem, because the canopy experiences strong structural changes with time.

The main objective of this study was to develop reliable approaches for the monitoring of green LAI *over complete rotations* of eucalypt plantations. For this purpose, we used a RTM, which has the advantage of taking into account changes in canopy structure and biochemistry with time. An original aspect of our methodology was the inversion procedure, which was constrained using a series of sigmoid curves to describe the time course of LAI. We compared these results with a simpler methodology based on vegetation indices. The specific objectives were therefore to (i) invert a RTM to estimate the LAI on one to seven years of MODIS reflectance time series of several stands, (ii) validate these LAI estimations with field measurements, (iii) compare the applicability and the performance of the RTM inversion approach with those of a simple vegetation index method, and (iv) analyse the uncertainty of both methods, and gain insight into the variables that are important for LAI estimations by means of a sensitivity analysis.

Section 2 gives an overview of the "biological" and radiometric data that were used, Section 3 describes the RTM, the inversion methodology, the vegetation index calibration and the uncertainty and sensitivity analysis procedure, and Section 4 presents the results. Section 5 discusses the objectives presented above in the light of the results, and offers some perspectives for future studies.

2. Data

2.1. Study site and stand selection

Eucalyptus plantations occupied approximately 4.3 million ha in Brazil in 2008 (ABRAF, 2009). In typical plantation management, soil is prepared with mechanical disking and harrowing a few months after each clear-cut harvest. New cuttings or seedlings are planted in rows at a density of ~1300 trees ha^{-1} and fertilized, and chemical weeding is carried out during the first year of growth. Harvesting occurs about six to seven years after planting, and foliage and branches are left on the ground. Leaf area index changes with stand age, with a maximum value generally attained during the second or third year. During the dry season, water stress causes a more or less marked seasonal decrease of LAI (up to ~50%), depending on soil water holding capacity and the age of the plantation.

Sixteen *Eucalyptus* stands belonging to the International Paper of Brazil Company, and two additional stands managed by the Duratex Company, were selected for our study in São Paulo State, south-eastern Brazil (Table 1).

The first 16 stands were planted with company-improved clones of *E. grandis* (W. Hill ex Maiden) * *E. urophylla* (S.T. Blake) hybrids and managed on six or seven-year rotations. The chosen stands were of different ages (aged 1 to 5 years) and productivity levels (30 to 53 m^3 commercial wood ha^{-1} yr^{-1}), but were genetically similar (commercial clone H13 and two stands of the closely-related clone H18) and exhibited very homogeneous canopies. They were larger than 30 ha and of compact shape. Eight stands were located close to the town of Brotas (28.22°S, 48.15°W, 647 m altitude), on relatively unfertile sandy soils (~90% sand, 8% clay, and 2% silt). The remaining stands were about 125 km east of Brotas in the vicinity of Mogi Guaçu (22.35°S, 46.97°W, 591 m altitude), on more fertile soils with a higher percentage of clay (~62% sand, 32% clay, and 6% silt).

The two Duratex stands were planted with *E. grandis* seedlings of a common controlled origin, and were 7 years old at the time of measurement. They presented contrasted productivity levels, as one stand (IT1) was planted on soil that was more fertile and clayey than that of the other (IT2) (see Table 1). These stands were part of the EucFlux Project experimental site close to Itatinga (22.97°S, 48.72°W, 740 m altitude).

The climate in the three zones is very similar, displaying a mean annual rainfall of ~1200 mm between 2000 and 2008 (ranging from 1044 mm in 2003 to 1345 mm in 2002). More than 80% of precipitation occurs during the wet season between October and April. Mean monthly air temperatures range from about 17 °C to 25 °C with an annual mean of 20 °C during the nine year period.

2.2. Destructive measurements of leaf biomass, LAI, and SLA

Three permanent inventory plots (400 m^2 each) were chosen in nine stands. The diameter at breast height (DBH, at 1.3 m above ground level) of each tree of the inventory plot was measured. These measurements were conducted 1) in order to ensure that trees for destructive measurements (chosen outside the permanent inventory plot) were sampled across the range of tree sizes, and 2) to enable upscaling of tree leaf area and other characteristics to the plot level with empirical models based on DBH (Fig. 1). Destructive sampling was carried out at two dates in 2008, on 7 stands during the wet season, close to the seasonal peak of LAI, and on 9 stands at the end of the dry season, when LAI was low. Four additional measurements were made at IT1 and IT2 stands in the 2007 and 2008 dry seasons and 2008 and 2009 wet seasons

Table 1
Characteristics of the 18 sampled stands. Stands marked with * are clone H18 (*E. grandis* * *E. urophylla*), with ** are seeds of *E. grandis*, others are clone H13 (*E. grandis* * *E. urophylla*); MAI7: estimated mean annual increment at year 7; HP: hemispherical photography; W. S.: wet season; D. S.: dry season.

Stand	Zone	Area (ha)	Estimated MAI7 of current crop (m^3 ha^{-1} $year^{-1}$)	Plantation date (of current crop)	Age on 01/04/2009 (year)	Destructive sampling date for LAI (DOY)				Sampling date of HP (DOY)	
						D. S. 2007	W. S. 2008	D. S. 2008	W. S. 2009	W. S. 2008	D. S. 2008
1 SF183U	Brotas	108.27	39.2	03/04/2007	2		94	260		94	263
2 SF178U	Brotas	93.12	41.4	29/03/2006	3.01		93	262		89	262
3 NS24U	Mogi Guaçu	108.53	41.4	04/04/2006	3			255		113	255
4 SF147	Brotas	49.93	39.3	15/05/2005	3.88					89	263
5 SF171	Brotas	48.7	40.6	05/05/2005	3.91		93	260		89	263
6 AB36	Mogi Guaçu	100.66	44.4	17/02/2005	4.12					115	274
7 SF43E	Brotas	65.52	32.5	06/05/2004	4.91		91	263		89	262
8 SF36E	Brotas	137.65	36.5	31/03/2004	5.01					116	262
9 MG14U	Mogi Guaçu	37.13	48.1	26/03/2004	5.02			254		86	254
10 MG16U*	Mogi Guaçu	42.07	45.9	17/12/2003	5.29					87	
11 NS101	Mogi Guaçu	42.74	43.7	18/10/2003	5.46					114	255
12 SF89	Brotas	40.31	30	11/06/2003	5.81		95	260		90	261
13 MG118	Mogi Guaçu	33.86	46.6	13/03/2003	6.06					87	274
14 G5E	Mogi Guaçu	37.45	40.6	08/05/2003	5.9					115	274
15 SF341*	Brotas	45.47	33.7	10/03/2003	6.07					90	261
16 P121	Mogi Guaçu	35.56	52.8	20/03/2003	6.04					114	
17 IT1**	Itatinga	40	40	06/03/2003	6.08	332	93	282	21		
18 IT2**	Itatinga	160	55	06/03/2003	6.08	332	93	282	21		

(see Table 1). LAI and stand-average specific leaf area (SLA, cm^2 g^{-1}) were estimated following the methodology described in Nouvellon et al. (2010) and detailed in Appendix A. Note that destructive sampling is generally considered as a very robust method for LAI estimations on these regular *Eucalyptus* plantations (Gower et al., 1999; Macfarlane et al., 2007), but is also time-consuming.

2.3. Crown cover

During the destructive sampling (date reported in Table 1), a relationship between DBH and maximum crown diameter was established for each sampled plot. This relationship was then applied to the permanent inventory plots to get the crown diameter of each tree. Tree crowns were considered to have a circular projected crown. Crown cover was then estimated as the fractional ground cover (comprised between 0 and 1) of the vertically projected crown area, calculated taking into account the spacing between trees and possible overlapping of neighbouring tree crowns. Note that this crown cover calculation did not take into account crown macroporosity, i.e. large gaps occurring within a tree crown. This assumption is coherent with the definition of crown cover of the RTM used in this study.

2.4. Leaf angle distribution

Leaf angles were measured during leaf biomass destructive sampling in the 2008 dry season (Appendix B). The up-scaled

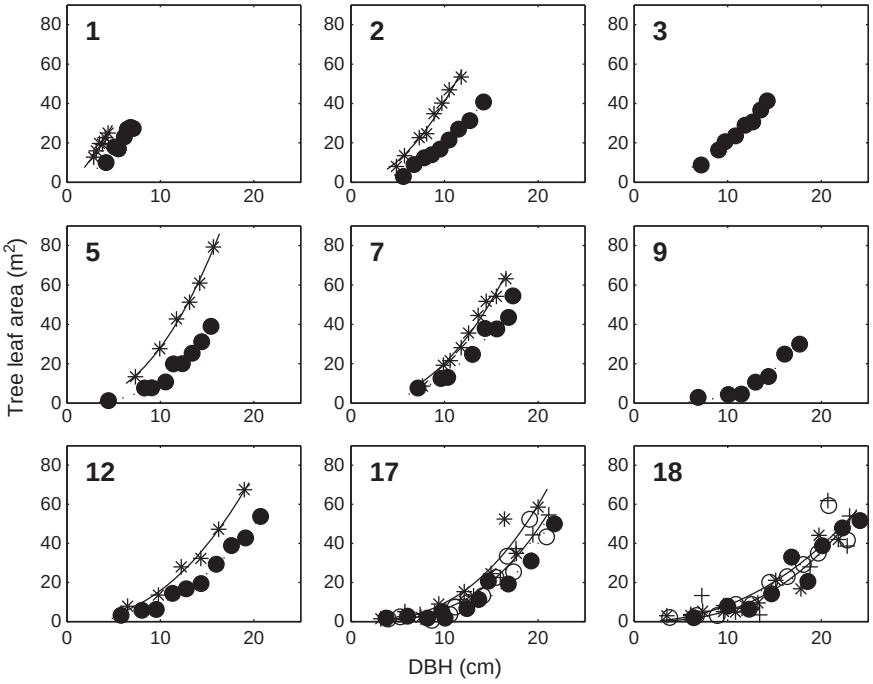

Fig. 1. Tree leaf area as a function of DBH for the nine stands of destructive LAI measurements (numbers relate to stand number in Table 1), for the 2008 wet season (stars) and 2008 dry season (closed circles). For stands 17 and 18, there are also measurements in the 2007 dry season (open circles), and 2009 wet season (cross). All power adjustments on clonal stands (see Appendix A Eqs. A1 and A2) have a R^2>0.92 and Root Mean Square Error<2.96 m^2. On the Itatinga stands (17 and 18), all R^2>0.78 and RMSE<10 m^2.

measurements of canopy leaf angle distribution were adjusted with a two parameter beta distribution function $f(\theta)$ (Goel & Strebel, 1984), which performs well on narrow and erectophile distributions such as those generally observed in *Eucalyptus* canopies (King, 1997):

$$f(\theta) = \frac{1}{B(u,v)}\left(1-\frac{\theta}{90}\right)^{\mu-1}\left(\frac{\theta}{90}\right)^{v-1}, \quad (1)$$

$$B(\mu,v) = \frac{\Gamma(\mu)\Gamma(v)}{\Gamma(\mu+v)}, \quad (2)$$

where μ and ν are two parameters, θ is leaf inclination angle in degrees, and Γ is the Gamma function.

2.5. Leaf reflectance

Leaf reflectance measurements were performed on three stands (SF183U, SF171 and SF89 in Table 1), and on approximately 50 leaves per stand. The leaf sampling scheme was stratified by tree size (three or four trees), height within the crown (three layers) and radial position of the leaves (four to eight positions). The reflectance and transmittance of the leaves were measured in the 450–900 nm spectral range with a SPECTRON SE-590, linked to a LICOR integrating sphere, like in Ponzoni and Goncalves (1999). The NIR and red spectral band reflectance and transmittance were calculated for each leaf using the MODIS relative spectral response of these bands (like in Asner et al., 1998).

2.6. Directional canopy gap fraction

Canopy gap fractions (GF) as a function of viewing angle were estimated with hemispherical photography at most of the stands (date of measurements reported in Table 1). The complete description of the methodology is given in Marsden et al. (2010). The gap fractions close to nadir (7.5°), 27.5° and 57.5° (within a +/−5° ring) were extracted and further used for comparison with the angular GF simulated by the inverted RTM.

2.7. Extraction of stand NDVI time series from MODIS images

2.7.1. Selection of the subset of MODIS pixels using high-resolution CBERS images

We used the MODIS/Terra MOD13Q1 products (Vegetation Indices 16-Day L3 Global 250m, Collection 5), which also contain 16-day red and near-infrared reflectances and sun and view angles.

The extraction of one MODIS reflectance time series per stand required the selection of pixels representative of the stand reflectance. Although each studied stand was large enough to encompass at least two MODIS pixels (Table 1), direct averaging of their reflectance was not appropriate because MOD13Q1 is a composite image, meaning that neighbouring pixels may have distinct acquisition dates and sun and view geometry. In addition, the position of the MODIS pixel is subject to uncertainties (Wolfe, 2006). The option we followed was therefore to select a single pixel to represent each stand. The selection involved checking how well the reflectance of the different candidate MODIS pixels compared with the whole-stand reflectance obtained from benchmark high-resolution images (details given in Appendix C). Note that for the largest stands, the use of the central pixel may be a valid and simpler option since stands are very homogeneous.

2.7.2. Extraction of MODIS data and filtering

A time series of 16 day MODIS vegetation indices was extracted (MOD13Q1 Vegetation Indices 16-Day L3 Global 250m, Collection 5) from early 2000 until March 2009. The MOD13Q1 data are already filtered from daily reflectance to keep the best vegetation index in a 16 day window. We excluded the pixels that did not have good NDVI quality and pixel reliability flags. The NDVI (Normalized Difference Vegetation Index) time series was corrected as in Soudani et al. (2008) for remaining outliers. In the end, about ~20% of the data were excluded. The red and NIR reflectances of dates where the NDVI was found to be correct were used afterwards.

3. Methods

3.1. Canopy reflectance model

Canopy reflectance is a complex result of leaf, soil and canopy structural properties. In this paper, the optical properties of these three components were simulated by PROSPECT4 (Feret et al., 2008), SOILSPECT (Jacquemoud et al., 1992) and 4SAIL2 (Verhoef & Bach, 2007). This is a good compromise between realism, computational speed, and number of input parameters despite the complexity of the studied system. We included a soil reflectance model to take into account directional effects. Another reason for the choice of these three submodels is that they are suitable for future coupling with SVAT models. We succinctly present here the three submodels.

The PROSPECT model (Jacquemoud & Baret, 1990) considers the leaf as a succession of absorbing layers. The new version PROSPECT4 (Feret et al., 2008) was found to perform better than previous versions of PROSPECT for *Eucalyptus globulus* leaves (Barry et al., 2009). PROSPECT4 calculates the leaf hemispherical reflectance and transmittance between 400 and 2500 nm with a 1-nm step as a function of leaf structure index (N_{struc}), leaf chlorophyll content (CHL, μg cm^{-2}), leaf water content (Cw, g cm^{-2}), and leaf mass per unit area (LMA, g cm^{-2}, inverse of SLA). Since the inversion of PROSAIL is done using red and NIR reflectances measured by MODIS-Terra, the 1 nm reflectance spectrum was averaged using the relative spectral response function of the MODIS-Terra red and NIR bands.

The 4SAIL2 model (Verhoef & Bach, 2007) is an improved version of the SAIL model (Verhoef, 1984). The SAIL RTM is a turbid-medium model that describes the canopy as a horizontally homogeneous layer, where leaves absorb, reflect, and transmit radiation. The radiative transfer equation is solved using an N-flux approximation: radiation is considered as four fluxes, diffuse and direct, upward and downward (Kubelka & Munk, 1931; Suits, 1972). The system is described by four differential equations for the four fluxes. In 4SAIL2, the representation of the canopy is changed by adding a vertically projected crown cover fraction (C_v) which represents inter-tree clumping. The LAI of the stand is calculated as the product of LAI_c and C_v, with LAI_c the leaf area index of the crown-projected surface of the stand. Green and brown leaves can be represented in 4SAIL2 as two sublayers, but in the case of eucalypt plantations, only green leaves are simulated since leaves fall shortly after yellowing. The leaf inclination distribution function used in this study is a beta distribution (Goel & Strebel, 1984) (see Eqs. 1 and 2).

SOILSPECT (Jacquemoud et al., 1992) simulates the bidirectional reflectance of a bare-soil from the angular response of the soil and an albedo value. It requires the single scattering albedo $\omega(\lambda)$, a roughness parameter (h), and four parameters (b, c, b', and c') for the phase function. In this study, we neglected the soil specular feature like in Weiss and Baret (1999), and therefore only b and c are used.

The coupled model PROSPECT + 4SAIL2 + SOILSPECT is called PROSAIL hereafter for sake of simplicity. The PROSAIL model input parameters are given in Table 2. The outputs of the model for this study are reflectance in two MODIS spectral bands, red and NIR. The coupled model is also able to simulate the canopy gap fraction as measured by hemispherical photography (i.e. considering the leaves as opaque) by setting leaf absorbance to 1 instead of using PROSPECT leaf reflectance and absorbance.

Table 2
Input parameters of the coupled PROSAIL model, with their default values, or the variable from which they are calculated in the inversion procedure.

Input parameter		Units	Constant value	Function of
PROSPECT 4				
N_{struc}	Leaf structure parameter		1.54	
Chl	Leaf chlorophyll content	$\mu g\ cm^{-2}$	55.0	
Cw	Leaf water content	$g\ cm^{-2}$	0.0145	
SLA	Specific leaf area	$cm^2 g^{-1}$		[Age, LAI]
4SAIL2				
LAI_c	Crown leaf area index	$m^2 m^{-2}$		Inverted
ν	Parameter of the beta LIDF			[Age]
μ	Parameter of the beta LIDF			[Age]
$s_{\prime}$	Hot spot size parameter		0.05	
f_B	Fraction brown leaf area	Unitless	0	
C_v	Vertical crown cover fraction	Unitless		[LAI_c]
ξ	Tree shape factor		0.28	
SOILSPECT				
h	Rugosity		0.47	
b	Parameter of the phase function		5.84	
c	Parameter of the phase function		−3.13	
ω_{red}	Soil albedo in red spectral band			[Site]
ω_{NIR}	Soil albedo in NIR spectral band			[Site]
Sun-object-sensor geometry				
θ_s	Solar zenith angle	°		[Site, Date]
θ_o	Observation zenith angle	°		[Site, Date]
ψ	Relative azimuth angle	°		[Site, Date]
s	Proportion of diffuse radiation	Unitless	0.4	

3.2. Model inversion

We inverted only the LAI, all other parameters being fixed to "measured" values, after preliminary tests highlighted that the use of only two bands, red and NIR, did not sufficiently constrain the inversion procedure to allow the retrieval of additional parameters. In these tests we inverted the RTM using the classical cost function which includes all variables, each with prior information (e.g. Combal et al. (2003)). Results showed that the prior value was chosen most of the time, whatever the prior boundaries chosen, meaning that an LAI value can be inverted for virtually any value combination of other variables. As a result, we preferred to fix all parameters but LAI to their well-determined "prior" values. A sensitivity analysis of the effect of these "prior" values on LAI retrieval is carried out in this study.

The inversions were carried out on entire rotations of eucalypt plantations. Because the time series covers about 9 years, we were able to invert the reflectance of the current crops since their planting date (maximum rotation length is about 7 years). The LAI varies inter-annually and seasonally throughout a rotation and its dynamics can be represented with a series of successive sigmoid curves. Two sigmoid curves per year allow the reproduction of foliage growth and leaf fall occurring in wet and dry seasons: if we assume that the probability of a leaf to grow or to fall is normally distributed around a date, then the cumulative probability has a sigmoid form (Clevers et al., 2002; Fisher et al., 2006). In reality, the probability distribution is not normal, and we accepted in our inversion procedure that sharp increases or decreases could occur (i.e. each sigmoid curve does not always reach its asymptotic value). This means that two successive sigmoid curves are joined in a common point, but at this point their first derivatives may be different. This is described by the following equation:

$$LAI_i(t) = LAI_{i-1}\left(t_{0,i}\right) + s \times \left(\frac{a_i}{1 + e^{\left(\frac{t_{0,i} + b_i - t}{c_i}\right)}} \right), \quad (3)$$

where i is the position number of the increasing or decreasing sigmoid curve which starts at $t_{0,i}$, and s takes the value $+1$ for periods of increasing LAI (wet season) or -1 for periods of decreasing LAI (dry season). The parameters a_i, b_i, c_i of the ith LAI sigmoid curve are adjusted to minimize the squared difference between all observed and simulated reflectances comprised between $t_{0,i}$ and $t_{0,i+1}$, using the Powell algorithm (Press et al., 1996). There are on average 9 reflectance values between $t_{0,i}$ and $t_{0,i+1}$. The value $LAI_{i-1}(t_{0,i})$ is obtained from the inversion of the previous sigmoid, apart from LAI_0 ($t_{0,1}$) which is set to zero.

The dates of limits between sigmoid curves, $t_{0,i}$, are fixed in the present study (one at the maximum and one at the minimum LAI of each year). Note however that the best date could be obtained automatically, but this procedure would require more computing time (see Discussion).

3.3. Model parameterization

The coupled PROSAIL model has many parameters listed in Table 2. In this study, we inverted the LAI_c (LAI of the crown cover). The canopy is very dynamic during a rotation, and therefore many structural and biophysical characteristics, if not all, can be expected to vary with time. However, our measurements have shown that only 6 parameters vary significantly between our experimental stands (LAI_c, SLA, μ, ν, C_v and soil albedo) and are therefore time-modeled. Other parameters were therefore considered constant in time and between sites (Table 2).

3.3.1. Leaf parameters

In the one-layer PROSAIL model, PROSPECT4 simulates the reflectance and transmittance of an "average leaf". The PROSPECT model is used instead of directly prescribing the measured leaf reflectance and transmittance into SAIL. This enables the simulation of leaf reflectance variation in response to variation of leaf parameters. Among the four PROSPECT4 parameters, only the SLA was considered to vary in time (see the following discussion), and the others were fixed to constant values.

3.3.1.1. Cw, Chl and N_{struc}. Leaf water content (Cw) was variable between stands, but no tendency with age or season was found (average ± standard deviation: $0.0145 \pm 0.003\ g\ cm^{-2}$). In addition, red and NIR have negligible specific absorption in PROSPECT.

Chlorophyll content (Chl) was not directly measured. These plantations are well fertilized, leading us to hypothesize that leaf chlorophyll content is not affected by nitrogen limitation and does not change much with stand age. This hypothesis is corroborated by the fact that measured leaf nitrogen content varied little between stands ($23.11 \pm 1.45\ g\ kg^{-1}$). In addition, leaves fall shortly after yellowing. For these reasons the chlorophyll content Chl was considered constant in the inversion procedure. The leaf structure parameter (N_{struc}) is not directly measurable but needs to be inverted. We therefore inverted the N_{struc} and Chl variables of PROSPECT4 model on the measured leaf reflectances and transmittances, while SLA and Cw were fixed to their measured values. Inversion showed good results, i.e. simulated and measured reflectance and transmittance were very similar (not shown). The inverted N_{struct} and Chl were not significantly different between stands (1.54 ± 0.03 and $55.0 \pm 6.3\ \mu g\ cm^{-2}$, respectively), and their mean inverted values were fixed in the model (Table 2). These values are in accordance with other studies on *Eucalyptus* species (Barry et al., 2009; Pinkard et al., 2006).

3.3.1.2. SLA. SLA measurements were significantly different between stands and were significantly correlated with measured leaf reflectance and transmittance in the NIR region. Measured SLA decreased with increasing stand age. This result is coherent with results presented by Almeida et al. (2004) for *Eucalyptus grandis* plantations.

They used a Gaussian function with a non-zero asymptote to fit the SLA versus age relationship, as did Sands and Landsberg (2002) for *E. globulus*. Our results on a few stands show that the shape of the model proposed by these studies fits well with our data (Fig. 2 and Eq. 4a and b). Stand-average SLA also varied seasonally (Nouvellon et al. 2010, for a *Eucalyptus urophylla*×*E. grandis* hybrid in Congo), with the lowest SLA values occurring at the end of the dry season, when LAI was the lowest, and highest SLA values occurring during the wet season near peak LAI. This was confirmed on our stands (Fig. 2). Seasonal variations of SLA were therefore assumed to follow the seasonal variations of LAI, but yearly minimum and maximum SLA, SLA_{min} and SLA_{max} ($cm^2\ g^{-1}$), were determined as a function of stand age (years):

$$\begin{cases} SLA_{min}(t) = SLA_{1,min} + \left(SLA_{0,min} - SLA_{1,min}\right) \times e^{-\log(2)\times\left(\frac{age(t)}{t_{SLA,min}}\right)^2} & \text{(a)} \\ SLA_{max}(t) = SLA_{1,max} + \left(SLA_{0,max} - SLA_{1,max}\right) \times e^{-\log(2)\times\left(\frac{age(t)}{t_{SLA,max}}\right)^2} & \text{(b)} \\ \text{if}(s=1),\quad SLA(t) = SLA_{min}(t) + (SLA_{max}(t) - SLA_{min}(t)) \times \frac{LAI(t) - LAI\left(t_{0,i}\right)}{LAI\left(t_{0,i+1}\right) - LAI\left(t_{0,i}\right)} & \text{(c)} \\ \text{if}(s=-1),\quad SLA(t) = SLA_{min}(t) + (SLA_{max}(t) - SLA_{min}(t)) \times \frac{LAI(t) - LAI\left(t_{0,i+1}\right)}{LAI\left(t_{0,i}\right) - LAI\left(t_{0,i+1}\right)} & \text{(d)} \end{cases} \quad (4)$$

where SLA_0 and SLA_1 are the SLA at age zero (planting), and for an old plantation, respectively; s takes the value +1 for periods of increasing LAI (wet season) or −1 for periods of decreasing LAI (dry season); LAI(t) is the LAI at time t, LAI($t_{0,i}$) and LAI($t_{0,i+1}$) are the LAI at the beginning or at the end of the inverted section i for an increasing LAI sigmoid curve (and opposite for a decreasing sigmoid curve). Note that the inversion method allows the determination of LAI($t_{0,i}$) and LAI($t_{0,i+1}$) for each date t. Fitting Eq. (4a and b) to our dataset (Fig. 2) resulted in $SLA_{0,min,} = 95\ cm^2\ g^{-1}$, $SLA_{1,min} = 70\ cm^2\ g^{-1}$, $t_{SLA} = 1.76\ year^{-1}$, and $SLA_{0,max} = 110\ cm^2\ g^{-1}$, $SLA_{1,max} = 85\ cm^2\ g^{-1}$, $t_{SLA,max} = 1.21\ year^{-1}$.

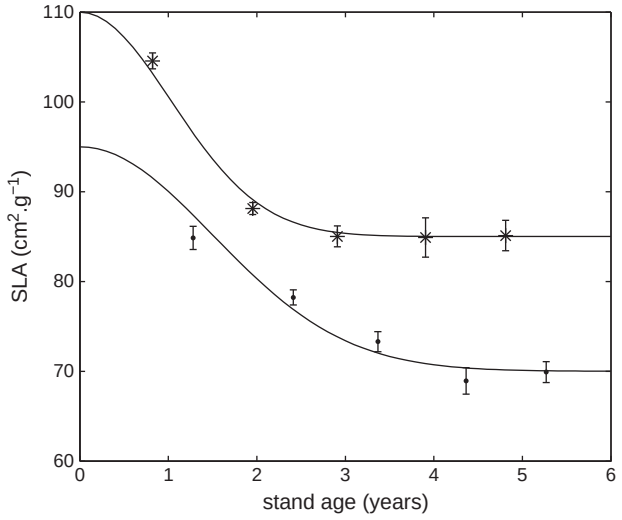

Fig. 2. Age-related variations of SLA: SLA measured at peak LAI during the wet season (SLA_{max}; stars), and SLA measured at the end of the dry season (SLA_{min}; filled circles). Black lines are simulated maximum and minimum SLA (Eq. 4). Simulated SLA fluctuates between these lines depending on LAI (Eq. 4).

3.3.2. Canopy parameters

The parameters of the beta distribution (Eqs. 1 and 2) of stand leaf angle distributions showed a clear trend with age (Fig. 3). We therefore simply used linearly interpolated values of ν and μ as a function of stand age in the inversion procedure.

The ratio of crown cover to crown-projected LAI_c was found to be very similar between stands in our measurements, and not dependant on stand age. We therefore fixed this ratio during the inversion procedure to the measured value (ratio of 0.167), with a maximum theoretical value of $C_v = 1.0$. The hot-spot size parameter was fixed to a constant value of 0.05 according to Verhoef and Bach (2007). The tree shape factor (crown diameter/height) was also stable with time and between measured stands (0.28 ± 0.04).

3.3.3. Soil parameters

Bare-soil red and NIR reflectances were estimated as the reflectance measured during the short interval between a clear-cut and the start of growth of the new rotation. This period lasts approximately two to three months, during which soil tillage and weed control occur. The 2000–2009 time series included at least one such inter-rotation period for each stand, and 2 in the case of the youngest sampled stands, thus giving 4 to 18 soil reflectance pairs per stand. When soil NIR reflectance was plotted against soil red reflectance, data points of each stand were arranged in a line, called the soil line.

Inversions of the SOILSPECT model on the bare-soil reflectances of each stand (representing 3 main soil types) showed that the rugosity and phase function parameters of SOILSPECT could be considered to be spectrally, spatially and temporally constant. Although some variability was observed between stands, it was not explained by soil type (ANOVA results $p = 0.468$). This inter-stand variability was therefore assumed to be the consequence of the scarcity of bare-soil data for some stands, of residual errors in reflectance or of some sparse herbaceous vegetation remaining after the clear-cut. The average values of rugosity and the two phase parameters are 0.47, 5.84 and −3.13 respectively (Table 2). These hypotheses are in accordance with Jacquemoud et al. (1992) and Privette et al. (1995) and correspond to the methodology adopted by Nouvellon et al. (2001). Conversely, the albedo parameters are expected to vary temporally, and to depend on the wavelength considered. The variation of red and NIR soil reflectances along the soil line is mainly due to single scattering albedo, which comes from changes in soil surface humidity (Jacquemoud et al., 1993), and to the amount of

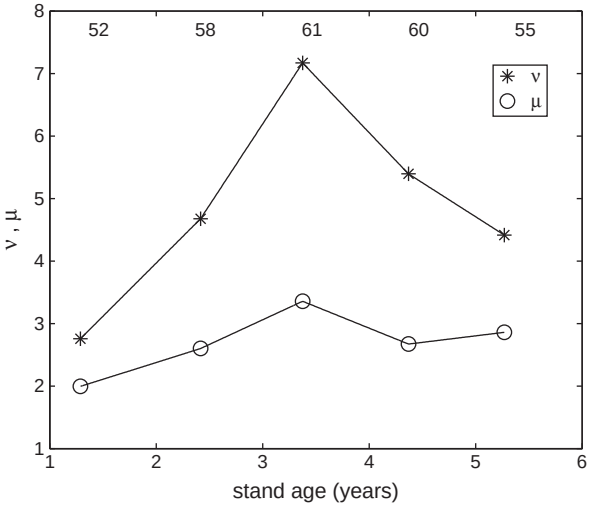

Fig. 3. Variations of the two parameters of the beta distribution (Eqs. 1 and 2) of leaf angle distribution function on stands of different ages. Average leaf angle (ALA), calculated as $ALA = 90(\nu/(\mu+\nu))$, is given for each stand.

litter present on the soil. View and sun geometries also participate in the scatter around the soil line. In this study, we do not have field measurements of soil albedo during the whole rotation, therefore the albedo was set to stand-specific values which were obtained from SOILSPECT model inversions on soil lines. Red albedo typically ranged from 0.10 to 0.16 and NIR albedo from 0.18 to 0.25.

3.4. Vegetation index

We chose to restrict our study to vegetation indices using only the red and NIR reflectance, i) as the other MODIS bands are measured at a lower spatial resolution, and ii) to allow a better comparison with the RTM inversion method. We tested the Simple Ratio, NDVI, SAVI and GESAVI indices, and the correlations r-square obtained with LAI were respectively 0.58, 0.58, 0.60 and 0.62. For the rest of the study we therefore used the Generalized Soil Adjusted Vegetation Index (GESAVI) (Gilabert et al., 2002).

$$GESAVI = \frac{NIR - a^{*}red - b}{red + Z} \quad (5)$$

The GESAVI index is based on the properties of LAI isolines in the NIR-red plane. For bare-soils (LAI = 0), the NIR and red reflectances are distributed along a line ($NIR_{soil} = a^{*}red + b$). When LAI increases, the NIR and red reflectances are distributed along a new line which intersects the soil line at $R = -Z$ and has a higher slope.

Based on the same soil reflectance dataset as that analysed above for SOILSPECT parameterization, we used a unique soil line with $a = 1.505$ and $b = 0.034$ (Fig. 4). For the sake of simplicity, the Z value was also considered constant ($Z = 0.0383$), even though it can in theory vary with vegetation cover (Gilabert et al., 2002). This Z value was chosen as the intersection of the soil line and the line of maximum LAI (see Fig. 4), with a simple visual line adjustment. Note that a sensitivity analysis of the Z parameter was conducted.

The GESAVI was further calibrated against measured LAI. A single linear relationship between LAI and GESAVI was assumed, and was used thereafter to obtain the time series of LAI from the time series of GESAVI. The LAI time series obtained from GESAVI was smoothed with a spline function to avoid artificial variations of estimated LAI due to residual atmospheric effects, view angle and noise in the reflectance data.

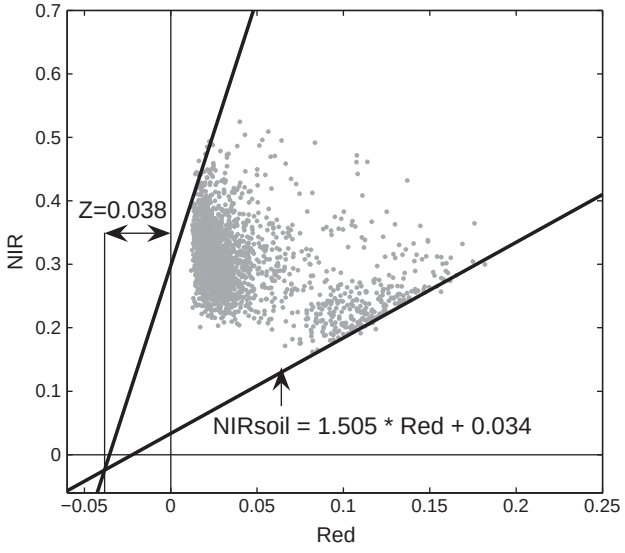

Fig. 4. NIR reflectance versus red reflectance for all stands listed in Table 1, for their entire rotation. This reflectance triangle was used to estimate the values of the GESAVI parameters. The soil line (corresponding to LAI = 0) is shown, together with an estimation of the value of parameter Z.

3.5. Uncertainty and global sensitivity analyses

The uncertainty and sensitivity analyses were conducted for the two LAI estimation approaches: (i) PROSAIL inversion and (ii) GESAVI-based method. These two methods are considered as "models", i.e. they have several inputs and one output, the retrieved LAI. The first model (PROSAIL inversion model) has 17 input variables, which include the parameters and variables listed in Table 2 and the MODIS red and NIR reflectances. The output is the (inverted) LAI. The second model (GESAVI-based LAI retrieval) has 5 input parameters and variables, which are given in Eq. (5), including red and NIR reflectances. Note that this model includes the smoothing of the LAI time series.

For each approach, the analyses aimed (1) to assess the uncertainty on estimated LAI and (2) to determine which variables most influenced the estimation of LAI, as a function of stand age and season.

We used the FAST method (Saltelli & Bolado, 1998; Saltelli et al., 1999), implemented in SimLab 2.2 (SIMLAB, 2009) to perform the uncertainty and sensitivity analyses. This method, based on Monte-Carlo sampling, allows both the estimation of the uncertainties and the determination of the first order and total effects of model parameters. The standard deviation of the output is a measure of the uncertainty of the model. The first order sensitivity index is a measure of the relative part of the total variance due to the simple effect of an individual input alone, acknowledging all other input variables. In this way, errors can be decomposed into component errors due to each of the input parameters, allowing the determination of the input parameter that has the highest sensitivity in the model. The total order sensitivity index is a measure of the relative importance of an input variable alone or in combination with other input variables.

We used a set of N combinations of input parameters ($N = 5\ 10^4$ for the first method and 10^4 for the second), by randomly selecting the input parameters. In order to be conservative in the uncertainty assessment, a uniform distribution was assumed for all parameters, with a range of variation of 10% around their prescribed average values or computed values, except reflectance values which were given a 5% range of variation. Due to the computational demand of such a calculation, this analysis was conducted on a single five-year-old stand (stand no. 12 SF89). Since the sensitivity can change with time (season and age), the analysis was carried out on a complete rotation.

4. Results

4.1. PROSAIL inversion and GESAVI index results

When LAI estimations are plotted against measurements, the correlations are high for both the PROSAIL and the GESAVI-based methods (R^2 of 0.80 and 0.62, respectively) (Fig. 5). The correlation coefficient is higher with the inversion method, but not statistically different. The PROSAIL inversion method results in very slight bias and a low RMSE, whereas the GESAVI tends to overestimate low LAI and underestimate high LAI. Note that the higher RMSE of the GESAVI method (0.52 compared to 0.41 for PROSAIL inversion) is largely due to the contribution of the highest measured LAI value.

The correlations are still significant when dry and wet season measurements are considered separately (R^2 of 0.77 and 0.45 respectively, for the PROSAIL method and R^2 of 0.48 and 0.39 for the GESAVI method), which means that the correlation is not only due to LAI seasonal variations which increase the LAI range, but also to interannual or inter-stand variations for a given season.

The inversion methodology was also tested using gap fractions measured with hemispherical photography, on a greater number of stands (Table 1). The determination coefficient of simulated and

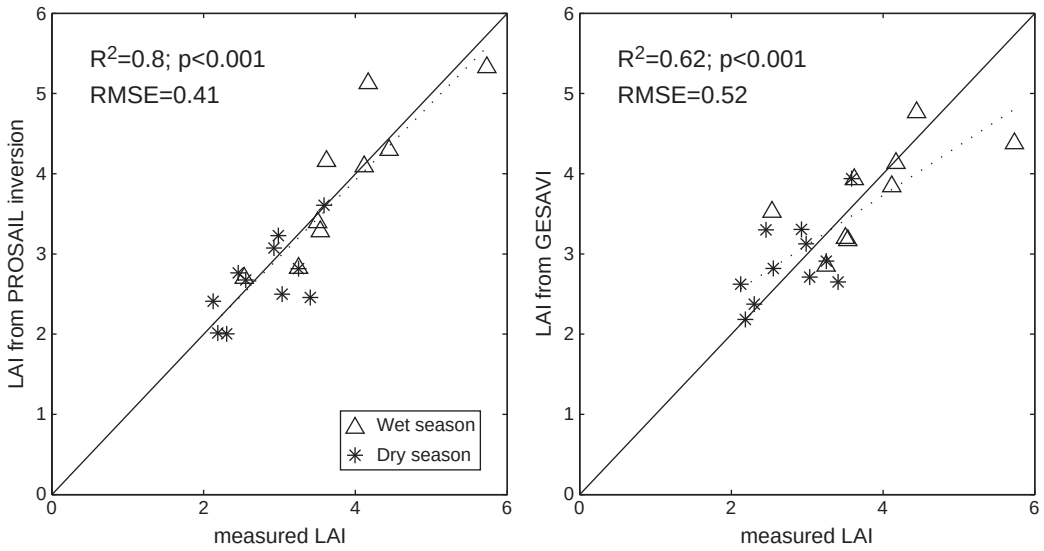

Fig. 5. Comparison of measured and estimated LAI from PROSAIL inversion (left) or from GESAVI (right). Measured LAI was obtained from destructive sampling.

measured GF is 0.56 for the three angles considered (Fig. 6). The correlations for each angle are also significant, and the bias is low.

Fig. 7 presents the LAI values estimated by PROSAIL inversion and using the GESAVI index during entire rotations. Typical LAI dynamics consist in a rapid increase of LAI during the first and sometimes second year of growth. The LAI then fluctuates seasonally, but generally maintains a high value (around 3–4). The seasonal variations are mainly due to the dry season, and show different shapes between years. General trends of LAI dynamics with age are variable between stands (see Discussion).

The residuals of the regression between measured LAI and LAI estimated by PROSAIL inversion show no bias with stand age (Fig. 8). In contrast, the residuals of LAI estimations from the GESAVI are all positive for stands younger than three years, which means that the LAI is generally overestimated. It is noticeable in Fig. 7 that LAI estimated from the GESAVI is higher than LAI estimated with PROSAIL inversions for ages lower than 3.

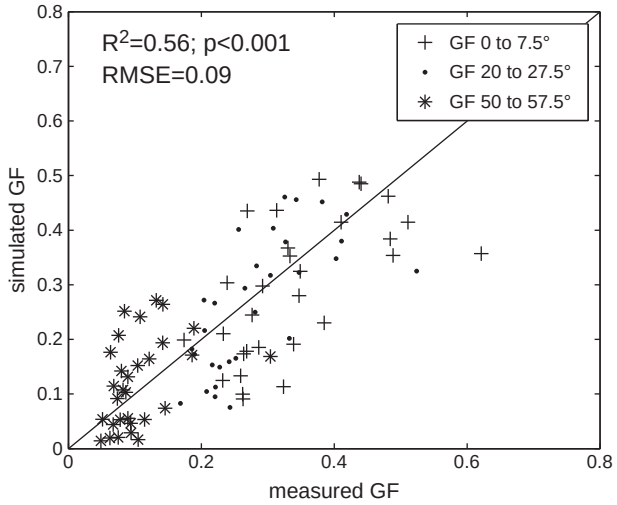

Fig. 6. Gap fraction (GF) simulated by PROSAIL after model inversion versus GF measured by hemispherical photographs, at three different view zenith angles and on 16 stands. Shown values of R^2 and RMSE are for all the data pooled. Regressions per view angle are also all significant at $p<0.05$.

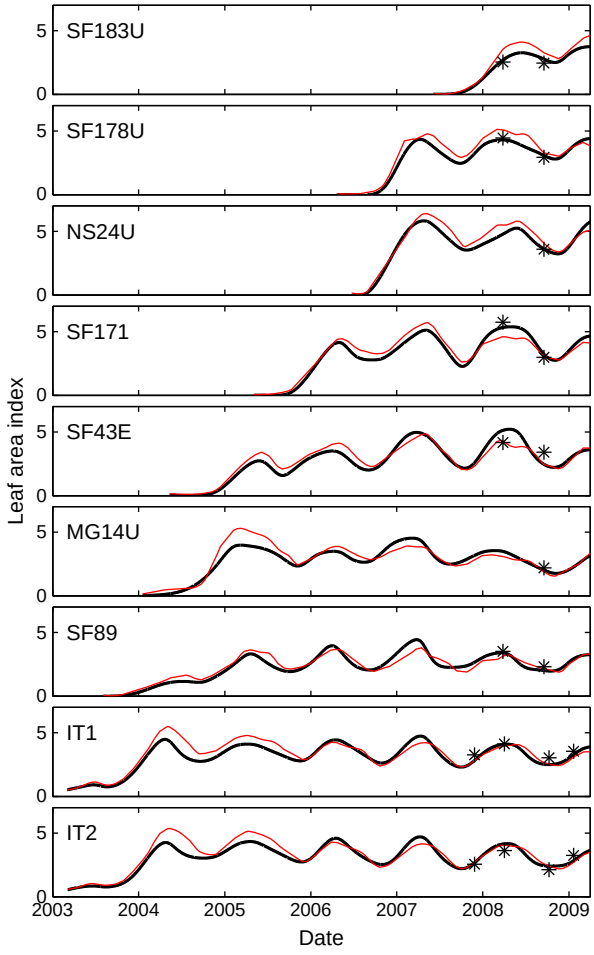

Fig. 7. LAI time series at 9 stands where LAI was measured by destructive sampling: LAI estimated from PROSAIL inversions (thick black lines) or from GESAVI (red lines). Stars indicate the value of LAI obtained from destructive measurements.

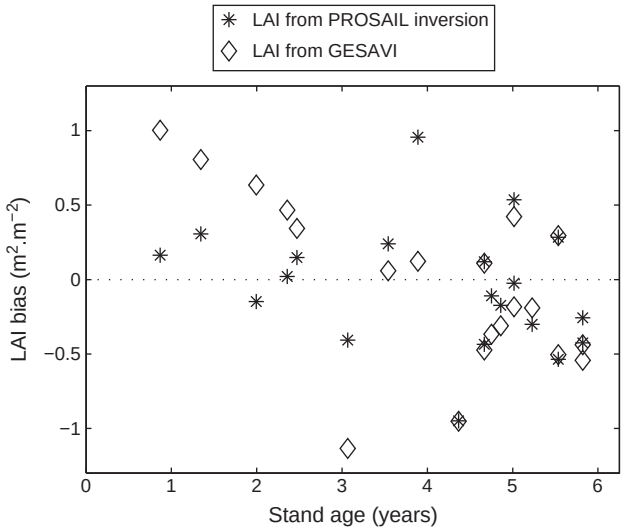

Fig. 8. LAI residual bias (difference between simulated and measured LAI) versus stand age, for the two methods of LAI estimation.

4.2. Uncertainty and global sensitivity analyses

Uncertainty in LAI values varies throughout the rotation with both methods (top plots of Figs. 9 and 10). The variance increases with the LAI, meaning that the uncertainty is higher for high LAI estimates. Our results show that the standard deviations are around 0.2 on average for both methods. The average results calculated with the Monte-Carlo runs are very close to the results of the simulation performed with the average input parameter values given in Table 2 (see Fig. 7).

Next we analysed the contribution of each parameter or variable to model uncertainty. In the case of the PROSAIL inversion method (Fig. 9), some parameters are hardly sensitive in the model (s, c, h, ξ, s_{ℓ}, Cw, and Chl), whereas others have substantial effects in the explored parameter space. We can therefore reduce the 17 input parameters to 10 uncertain parameters. Moreover the sum of all parameter indices is close to 1, which means that the total output variance is mainly due to single parameter effects, and not to combined effects (total effect sensitivity indices not shown). Some input parameters are more important at the beginning of the rotation and when the LAI is low (soil albedo explains around 60% of the output variance at this point), while others are more important when the LAI is high (C_v, SLA and ρ_{NIR}). Overall, we can see that the LAI is mainly sensitive to soil albedo at the beginning of the rotation (age<1 year) and to more temporally variable parameters for the rest of the rotation. When we look at PROSAIL submodels, we can see that (i) the PROSPECT model has only a small influence, (ii) the SOILSPECT model is sensitive throughout the rotation, but mainly when LAI is low, (iii) 4SAIL2 is sensitive whenever LAI>1, and finally, and not surprisingly, (iv) the red and NIR reflectances are sensitive throughout the entire rotation.

For the GESAVI method (Fig. 10), there is no interaction effect between input parameters, therefore the sum is exactly one during the entire rotation. The b parameter is not sensitive in the model. The parameter a is sensitive at the beginning of the rotation compared to the other parameters. The parameter Z is very sensitive from the age of about one year till the end of the rotation. Finally, most of the total variance of the output is due to reflectance values, which explain about 60% of the total variance. It is important to underline that these sensitivity analysis results are relevant for the specific case of a eucalyptus plantation of a given age, with the restricted parameter space detailed above.

5. Discussion and perspectives

The parameterization of the reflectance model is tricky for the inversion of the LAI on a complete rotation. The canopy is highly

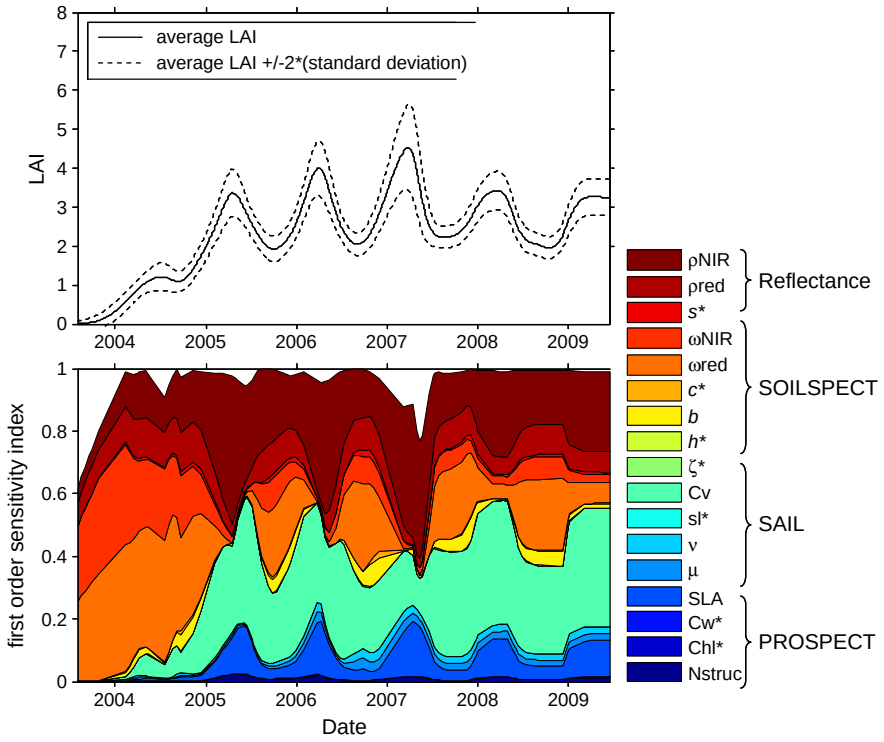

Fig. 9. Uncertainty and global sensitivity analysis of PROSAIL inversion for stand no. 12 SF89. Top: LAI average values, and two standard deviations, an estimate of the uncertainty in the LAI estimation resulting from a 10% uncertainty in the input parameters (5% for reflectances). Bottom: stacked area of first order sensitivity indices of all PROSAIL input parameters (see Table 2 for their description) computed with the FAST algorithm. (*): input parameters that have quasi-null first order sensitivity index.

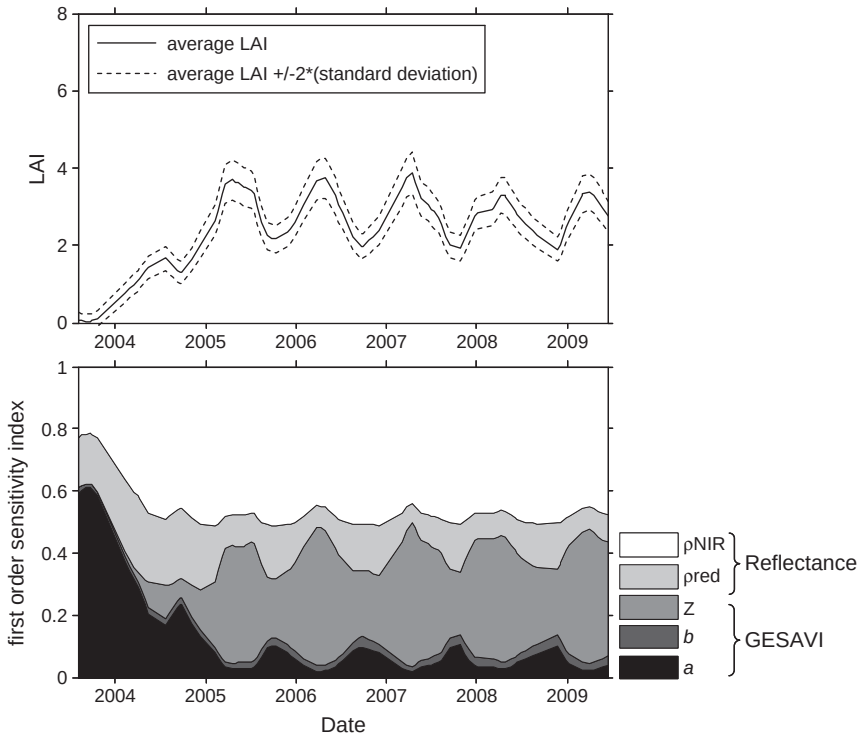

Fig. 10. Uncertainty and global sensitivity analysis of the GESAVI-based method for stand no. 12 SF89. Top: LAI average values and two standard deviations, an estimate of the uncertainty. Bottom: stacked area of first order sensitivity indices of all GESAVI input parameters and reflectances, computed with the FAST algorithm.

dynamic and many inputs of the model vary during the rotation. In the present study, we took into account most of these changing parameters using information derived from field data. However, the necessary field measurements are labour-intensive, and therefore we relied on a small set of measurements. More field work on different ages, soil types and at different seasons would help to improve the parameterization procedure.

The low uncertainty obtained in the uncertainty analysis is probably underestimated since a 10% variation may be low for some input parameters, and structural errors were not accounted for. The uncertainty analysis showed that the higher the LAI, the higher the uncertainty on the value. This comes from two effects: the effect of a proportional error on NIR reflectance, but also the saturation effect of indices and models for high LAI. This conclusion means that efforts towards the reduction of the overall uncertainty on LAI estimations should focus first on periods where the LAI is high (above ~3), which is a common challenge in forest LAI estimation (Fassnacht et al., 1997; le Maire et al., 2006; Soudani et al., 2006). During these periods (second half of the wet season), the most sensitive parameters are C_v and SLA. The measurements should therefore focus on these parameters (and on LAI_c). Other important parameters are soil albedo and leaf angles.

The SOILSPECT model was sensitive throughout the entire rotations, but was particularly important at the beginning and during dry seasons (Fig. 9, bottom). This oscillating pattern is due to the interaction between variations of C_v and variations of LAI_c, as these variables are correlated in the inversion procedure. More effort is necessary to separate crown cover from LAI_c in order to estimate the stand-average LAI. For this purpose, very high-resolution images could be used to estimate the vegetation cover from linear spectral unmixing, like in Goodwin et al. (2005). In the parameterization of SOILSPECT, we fixed the soil albedo to a stand-specific constant value. Our hypothesis of a constant albedo with time is supported by observations of similar MODIS soil reflectance values before and after the rotation of certain stands. However, the soil reflectance measured in the inter-rotation period may be different from that of the forest floor during the rest of the rotation, because of variability in soil moisture and gradual changes in litter quantity and composition. This effect could be investigated by measuring the soil albedo of one stand continuously to follow its temporal variation during a rotation.

Despite the uncertainties on the measurements, and the different assumptions of the PROSAIL model we used, the inversions showed good results, with an R^2 of 0.8 and a RMSE of 0.41 $m^2\ m^{-2}$. Moreover, the model was able to estimate the highest measured LAI values of 4 to 6 $m^2\ m^{-2}$, and gave good results during both wet and dry seasons. Finally, the inverted RTM was shown to represent correctly, on average, the canopy gap fraction at different angles. The LAI (and GF) measurements to which the model results are compared may also suffer from uncertainty due to measurement methodology and spatial variability. In particular, the scattering of the GF in Fig. 6 may arise partly from the difficulties associated with their estimation by hemispherical photography (as discussed in Marsden et al., 2010), and from the spatial variability within a plot, which is not accounted for in the RTM.

A drawback of the use of sigmoid curves is that real-time estimations of LAI cannot be made, since whole half-years of data (between the dates of maximum and minimum yearly LAI) are needed for model inversion. However the use of a sigmoid curve in the inversion procedure presents several advantages: (i) it produces a smoothed LAI time series, which is consistent with the gradual production and shedding of leaves (ii) it reduces residual errors on reflectance due to atmospheric corrections, bad pixel quality, etc. (iii) it allows the use of the minimum or maximum seasonal value of LAI for computation of other parameters (e.g. SLA in Eq. 4), (iv) it is a direct source of phenological information (date of inflexion points), and (v) it offers the possibility of further constraining the inversion (e.g. limiting the maximum rate of LAI increase or decrease). The

sigmoid algorithm we have used here can be further improved by automatically finding the limits between sigmoid curves, or by avoiding sharp changes of LAI at transitions (Xiao et al., 2009).

The obtained LAI dynamics throughout a *Eucalyptus* rotation present a similar pattern to those reported in other studies (Almeida et al., 2004; du Toit, 2008; Stape et al., 2008). However, the decrease of LAI that is generally measured after 2–3 years in this type of plantation did not appear clearly here. These inverted LAI can be used in process-based models that simulate biomass growth of *Eucalyptus* stands, like 3PG (Landsberg & Waring, 1997) or G'Day (Comins & McMurtrie, 1993; Corbeels et al., 2005). This approach has shown some promising results for a better retrieval of stand biomass (le Maire et al., 2010). Another advantage of RTM is the possibility of tight coupling with such ecophysiological process-based models because they share a number of common variables (SLA, C_v, LAI, leaf biomass, etc.), and many processes of radiation transfer which are of first importance in process-based models (Viovy et al., 2001).

For the estimation of LAI only, the complexity of the RTM inversion led us to test a simpler and more practical approach based on a vegetation index. In this study, we used the GESAVI index, which explicitly takes into account the distance to the soil line. This index was shown to give good estimates of LAI, with an R^2 of 0.62 and a RMSE of 0.52 m^2 m^{-2} but showed some saturation for high LAI (although only one point shows this saturation). The LAI values obtained with the GESAVI were similar to those obtained with PROSAIL in terms of seasonal amplitude, but the index overestimated low LAI, and therefore biased the results at the beginning of the rotation. It also presented a small temporal shift, which could be due to a solar zenith angle effect on the GESAVI, that is accounted for in the RTM inversion. The smoothing step of the GESAVI methodology is very important since the GESAVI does not correct for acquisition geometry effects, and LAI values are not dynamically constrained as with the sigmoid curve method used in PROSAIL inversions. The GESAVI could be improved by developing an objective procedure for the determination of the *Z* parameter (adjusted visually in the present study), and by integrating a crown cover factor, as suggested in Gilabert et al. (2002), or an age correction factor. The soil line could also be separated by stand, to create a stand-specific GESAVI; this was not done in our study for the sake of simplicity.

This work can be the basis for further improvements of the GESAVI, or other vegetation indices, based on the LAI measurements and results from PROSAIL inversions. The LAI obtained by PROSAIL inversion can be considered as a good approximation of the true LAI, and can be used for vegetation index calibration. Index calibration could be performed using a simulated LAI-reflectance database that includes a broad range of image acquisition and stand configurations. This methodology has already been used for the calibration of chlorophyll content indices in leaves (le Maire et al., 2004) and canopies (Houborg et al., 2007; le Maire et al., 2008), and yielded robust indices, easy to apply at large scales. More complex models such as 3D ray-tracing models could improve the results, but are more difficult to parameterize and are computationally intensive. 3D models could however improve some particular aspects that are not taken into account here, such as the vertical gradient of leaf angle (Utsugi et al., 2006), SLA (O'Grady et al., 2008) and leaf area density (Medhurst & Beadle, 2001).

Finally, the methodology we developed aimed at obtaining the LAI over the complete rotation of several stands. In view of estimating the LAI of an entire forest (i.e. at the landscape/regional scale) over a decade, the methodology would require parameterization/calibration and testing on other clones and seedling plantations. In addition, reflectance time series would be needed for every stand in the forest, even those of small size.

This could be achieved through stand-scale unmixing of MODIS data (Zurita-Milla et al., 2009). Such an unmixing procedure, if it were applied to the 500 m resolution data in 7 bands of MOD09A1, would also allow the use of additional spectral bands in the inversion procedure, which could in this way be less tightly constrained and enable the estimation of more parameters.

6. Conclusion

Leaf area index time series of *Eucalyptus* plantations can be obtained on entire rotations, at the level of the stand, with a RMSE of 0.41 or 0.52 from radiative transfer model inversion or from a vegetation index-based method, respectively. The use of sigmoid functions to constrain the inverted LAI improved its estimation by including information about the time course of reflectance. Uncertainties in LAI estimations due to uncertainties in model parameters were found to be of the order of 0.2. RTM inversions proved to be more efficient but suffered from a difficult parameterization, which was not the case with the index-based method. The index-based method noticeably overestimated the LAI at the beginning of the rotation. We propose that further studies should focus on the improvement of the GESAVI index for a specific and simplified application on *Eucalyptus* rotations, for LAI estimations. This can be done by using the RTM to calibrate such an index, in addition to field measurements.

Acknowledgements

This study was funded by the European Integrated Project Ultra Low CO2 Steelmaking (ULCOS—contract no. 515960), by CNPq 306561/2007, and by the EucFlux project. We thank International Paper do Brasil and in particular José Mario Ferreira, Augusto Miguel Nascimento Lima and Sebastião Oliveira, for providing data and technical help for field campaigns, and the French Ministry of Foreign Affairs for their financial support. We are also very grateful to Osvaldo Cabral (EMBRAPA), Marcos Ligo (EMBRAPA), Elcio Reis (IPBr), Cristiane Camargo Zani (ESALQ), Giampiero Bini Cano (Instituto Botanico), Renato Meulman Leite da Silva (ESALQ), and Reinaldo Camargo (ESALQ) for their help during field work. We thank the anonymous reviewers for their helpful advice and valuable comments on how to improve the manuscript.

Appendix A. Destructive measurements of leaf biomass, LAI and SLA

After the inventory, the diameter distribution was divided into 6 to 12 classes, and one tree of corresponding DBH was selected at random in each class (outside but close to the permanent plots). The tree was then felled and the green crown length was divided into three equal-length parts (lower, middle and upper). All leaves of each part were removed and weighed immediately (total fresh mass). Twenty-five leaves were randomly selected in each part and kept cold until their fresh mass and area were determined in the laboratory. These leaves were then dried at 65 °C till constant weight, and fresh to dry mass ratios were calculated. The leaf area of each crown section was calculated by multiplying the surface to fresh mass ratio (calculated on the 25 sampled leaves) by the total fresh mass.

Single-tree leaf area (A_t) and leaf biomass (B_t) were computed as the sum of the leaf area (for A_t), or leaf biomass (for B_t) of the three crown parts. Allometric relationships were then established between A_t and DBH (Fig. 1), and between B_t and DBH (not shown), for each stand and each date, and were applied to the DBH measurements of the inventory plots, to estimate the plot-average LAI and SLA:

$$LAI_p = \frac{\sum_{i=1}^{n} a_A DBH_i^{b_A}}{A_p}, \quad \text{(A1)}$$

$$SLA_p = \frac{\sum_{i=1}^{n} a_A DBH_i^{b_A}}{\sum_{i=1}^{n} a_B DBH_i^{b_B}}, \quad \text{(A2)}$$

where n is the number of trees in the inventory plot, DBH_i is the measured DBH of the ith tree, A_p is the area covered by the plot, and a_A, b_A, and a_B, b_B are the fitted parameters of the power functions relating A_t to DBH (e.g. Gower et al., 1999), and B_t to DBH, respectively. These calibrated functions give very precise estimates of A_t and B_t for these clonal eucalypt plantations (Fig. 1; and see also Nouvellon et al., 2010). Finally, the estimated values of LAI_p and SLA_p of the three inventory plots were averaged to derive the values of the stand-average LAI and SLA.

Appendix B. Leaf angle distribution measurements

We selected four to five trees of contrasted sizes per stand among the ones sampled for destructive LAI measurements. The inclination angle of 60 leaves per tree was measured, stratified by 3 crown sections (bottom, middle, and top), 4 different branches in the 4 azimuth directions, and five leaves along each branch. The inclination angle of each leaf was measured on the principal leaf blade axis with a protractor and a plumb line. On each stand, leaf angles showed a clear trend with height of the measured leaves whatever the position within the crown of the sampled tree (Fig. B1): low leaves were more horizontal than high leaves. This relationship was used to scale the leaf angle distribution to the inventory plot. This was done by separating the canopy into about 20 horizontal layers. Leaf angles inside each layer were assumed to follow a normal distribution, with the mean and the standard deviation deduced from layer depth with a simple second order polynomial (relationships obtained from measurements, Fig. B1). The leaf area of each layer was calculated from destructive sampling scaled to the stand level. Finally, the leaf angle distribution of the entire canopy was calculated as the sum of the layer leaf angle distributions weighted by the layer foliage area.

Appendix C. Selection of the subset of MODIS pixels using high-resolution CBERS images

We used high-resolution China–Brazil Earth Resources Satellite CCD sensor (CBERS-2 CCD) images for each region (Brotas, Mogi Guaçu, and Itatinga) as a benchmark, to check that the reflectance of a MODIS pixel could be representative of mean stand reflectance obtained from 20 m resolution images. Among the MODIS pixels located within the boundaries of a stand, the most representative one was selected for the rest of the study. The selection procedure involved first manipulating CBERS-2 data to render it comparable with MODIS data, and then comparing CBERS-2 and MODIS reflectances at a range of dates, according to the following steps:

(1) All available cloud-free CBERS-2 images (i.e. 20 images per region between 2004 and 2008) were downloaded and geo-referenced, and the atmospherically corrected MODIS images (MOD09GQ Surface Reflectance Daily L2G Global 250m, Collection 5) of the same dates were also downloaded, or of the closest date if the same-date viewing angle was greater than 25°.
(2) The CBERS-2 digital counts (DC) were averaged to the MODIS grid. The resolution of the obtained data (hereafter referred to as CBERS-2-modres) exactly matched the MODIS pixel grid.
(3) We applied a linear fit between the CBERS-2-modres and MODIS reflectances for each date, both for red and for NIR reflectance. The correlation was generally very strong because the images were large enough to encompass a large range of reflectance values (median r-square of 0.86, minimum of 0.69 and maximum of 0.94 for the red band, and a median of 0.91, minimum of 0.70 and maximum of 0.96 for NIR, on the 54 CBERS-2 images used). The residuals of the regression were regularly distributed. The regression coefficients (gain and offset) were calculated for each spectral band of each CBERS-2 image.
(4) All CBERS-2DC of the native resolution (20 m) were corrected into MODIS-like reflectance using the gain and the offset calculated earlier (hypothesis of linearity of the correction), to

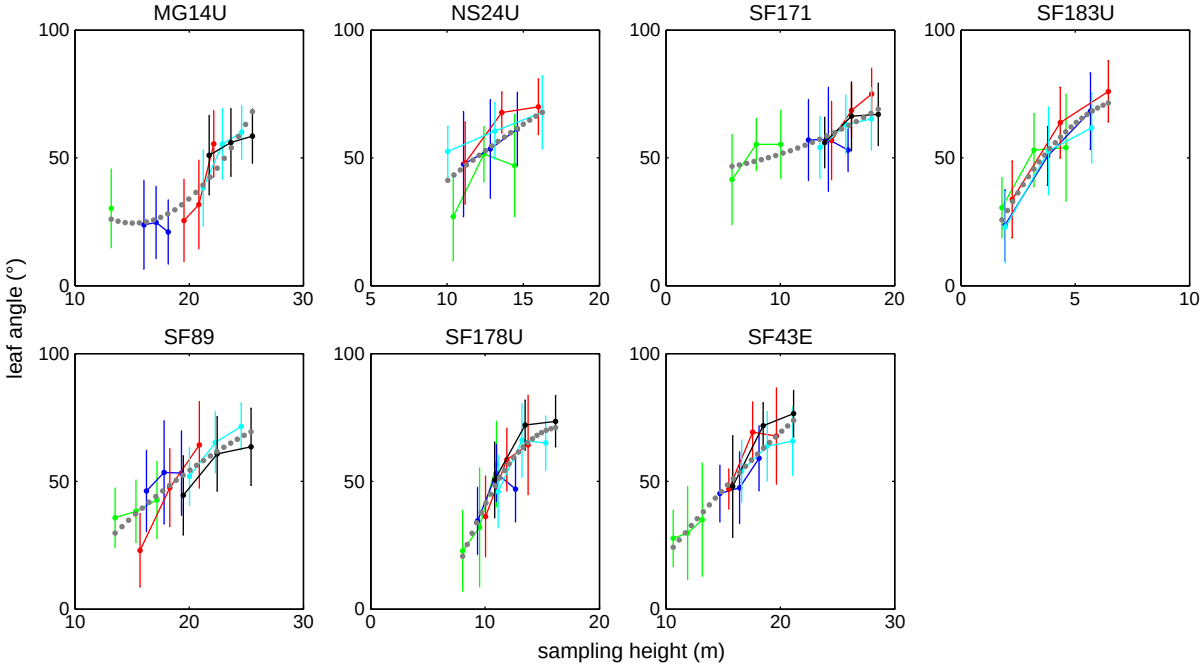

Fig. B1. Leaf inclination angles measured on different trees (colors) as a function of leaf sampling height. Leaf angles show a clear trend within the canopy, shown in grey dotted line.

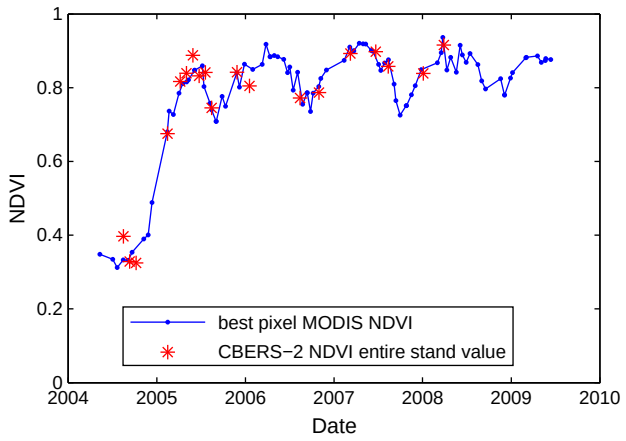

Fig. C1. NDVI time series of the best pixel found for SF43E stand, compared to the CBERS-2-modres NDVI time series for the entire stand.

obtain CBERS-2-corr. In this way, CBERS-2-corr included a correction of atmospheric effects and of other factors such as sun and view angles and relative spectral responses of the bands. The linearity of the correction between both images at MODIS resolution, and the normality of the distribution of residuals, allowed its application to the 20 m resolution CBERS-2 images for their correction. Note that the linear regression is extrapolated for extreme local values in the CBERS-2 image (which generally represented less than 1% of the image).

(5) The reflectance of each stand of Table 1 (with a 60 m buffer because of the Effective Instantaneous Field Of View, Bensebaa et al., 2008) was extracted from each CBERS-2-corr image. Average stand values were computed per band, which gave about 20 red and 20 NIR values per stand for the period between 2004 and 2008. MODIS pixels which were totally inside the stand delimitations were also extracted (from 2 to 8 pixels, depending on the size and shape of the stand). At this step of the procedure, we confirmed that the CBERS-2 reflectance of each stand was very homogeneous, with a median coefficient of variation of 0.08 for red and 0.03 for NIR (similar values for the MODIS coefficient of variation for stands including at least 3 pixels).

(6) For each MODIS pixel position, a linear correlation coefficient between the different-date MODIS reflectances and stand reflectances (from CBERS-2-corr) was calculated. If the correlation was high (r^2>0.85), the pixel was considered representative of stand reflectance.

(7) For each stand, the MODIS pixel which gave the highest correlation coefficient among the representative pixels was selected for further use in this paper (example given in Fig. C1).

References

ABRAF (2009). *Chapter 01, planted forests in Brazil.*Statistical Yearbook 2009.

Almeida, A. C., Landsberg, J. J., & Sands, P. J. (2004). Parameterisation of 3-PG model for fast-growing *Eucalyptus grandis* plantations. *Forest Ecology and Management*, *193*, 179−195.

Almeida, A. C., Soares, J. V., Landsberg, J. J., & Rezende, G. D. (2007). Growth and water balance of *Eucalyptus grandis* hybrid plantations in Brazil during a rotation for pulp production. *Forest Ecology and Management*, *251*, 10−21.

Asner, G. P., Wessman, C. A., Schimel, D. S., & Archer, S. (1998). Variability in leaf and litter optical properties: Implications for BRDF model inversions using AVHRR, MODIS, and MISR. *Remote Sensing of Environment*, *63*, 243−257.

Bacour, C., Baret, F., Beal, D., Weiss, M., & Pavageau, K. (2006). Neural network estimation of LAI, fAPAR, fCover and LAIxC(ab), from top of canopy MERIS reflectance data: Principles and validation. *Remote Sensing of Environment*, *105*, 313−325.

Baret, F., Hagolle, O., Geiger, B., Bicheron, P., Miras, B., Huc, M., et al. (2007). LAI, fAPAR and fCover CYCLOPES global products derived from VEGETATION: Part 1: Principles of the algorithm. *Remote Sensing of Environment*, *110*, 275−286.

Barry, K. M., Newnham, G. J., & Stone, C. (2009). Estimation of chlorophyll content in *Eucalyptus globulus* foliage with the leaf reflectance model PROSPECT. *Agricultural and Forest Meteorology*, *149*, 1209−1213.

Bensebaa, K., Banon, G. J. F., Fonseca, L. M. G., & Erthal, G. J. (2008). On-orbit spatial resolution estimation of CBERS-2 imaging system using ideal edge target. *Signal Processing for Image Enhancement and Multimedia Processing*, 37−48.

Clevers, J. G. P. W., Vonder, O. W., Jongschaap, R. E. E., Desprats, J. -F., King, C., Prévot, L., et al. (2002). Using SPOT data for calibrating a wheat growth model under Mediterranean conditions. *Agronomie*, *22*, 687−694.

Combal, B., Baret, F., Weiss, M., Trubuil, A., Mace, D., Pragnere, A., et al. (2003). Retrieval of canopy biophysical variables from bidirectional reflectance: Using prior information to solve the ill-posed inverse problem. *Remote Sensing of Environment*, *84*, 1−15.

Comins, H. N., & McMurtrie, R. E. (1993). Long-term response of nutrient-limited forests to CO_2 enrichment; equilibrium behavior of plant-soil models. *Ecological Applications*, *3*, 666−681.

Corbeels, M., McMurtrie, R. E., Pepper, D. A., Mendham, D. S., Grove, T. S., & O'Connell, A. M. (2005). Long-term changes in productivity of eucalypt plantations under different harvest residue and nitrogen management practices: A modelling analysis. *Forest Ecology and Management*, *217*, 1−18.

du Toit, B. (2008). Effects of site management on growth, biomass partitioning and light use efficiency in a young stand of *Eucalyptus grandis* in South Africa. *Forest Ecology and Management*, *255*, 2324−2336.

Fang, H., & Liang, S. (2005). A hybrid inversion method for mapping leaf area index from MODIS data: Experiments and application to broadleaf and needleleaf canopies. *Remote Sensing of Environment*, *94*, 405−424.

FAO (2006). Global planted forest thematic study: results and analysis. In A. Del Lungo, J. Ball, & J. Carle (Eds.), *Planted forests and trees working paper*, *38*, Rome, Italy.

Fassnacht, K. S., Gower, S. T., MacKenzie, M. D., Nordheim, E. V., & Lillesand, T. M. (1997). Estimating the leaf area index of North Central Wisconsin forests using the landsat thematic mapper. *Remote Sensing of Environment*, *61*, 229−245.

Feret, J. -B., François, C., Asner, G. P., Gitelson, A. A., Martin, R. E., Bidel, L. P. R., et al. (2008). PROSPECT-4 and 5: Advances in the leaf optical properties model separating photosynthetic pigments. *Remote Sensing of Environment*, *112*, 3030−3043.

Fisher, J. I., Mustard, J. F., & Vadeboncoeur, M. A. (2006). Green leaf phenology at Landsat resolution: Scaling from the field to the satellite. *Remote Sensing of Environment*, *100*, 265−279.

Gilabert, M. A., González-Piqueras, J., García-Haro, F. J., & Meliá, J. (2002). A generalized soil-adjusted vegetation index. *Remote Sensing of Environment*, *82*, 303−310.

Goel, N. S., & Strebel, D. E. (1984). Simple beta distribution representation of leaf orientation in vegetation canopies. *Agronomy Journal*, *76*, 800−802.

Goodwin, N., Coops, N. C., & Stone, C. (2005). Assessing plantation canopy condition from airborne imagery using spectral mixture analysis and fractional abundances. *International Journal of Applied Earth Observation and Geoinformation*, *7*, 11−28.

Gower, S. T., Kucharik, C. J., & Norman, J. M. (1999). Direct and indirect estimation of leaf area index, fAPAR, and net primary production of terrestrial ecosystems. *Remote Sensing of Environment*, *70*, 29−51.

Houborg, R., Soegaard, H., & Boegh, E. (2007). Combining vegetation index and model inversion methods for the extraction of key vegetation biophysical parameters using Terra and Aqua MODIS reflectance data. *Remote Sensing of Environment*, *106*, 39−58.

Jacquemoud, S., & Baret, F. (1990). PROSPECT: A model of leaf optical properties spectra. *Remote Sensing of Environment*, *34*, 75−91.

Jacquemoud, S., Baret, F., & Hanocq, J. F. (1992). Modeling spectral and bidirectional soil reflectance. *Remote Sensing of Environment*, *41*, 123−132.

Jacquemoud, S., Baret, F., & Hanocq, J. F. (1993). Modélisation de la réflectance spectrale et directionnelle des sols : application au concept de droite des sols. *Cahiers ORSTOM. Série Pédologie*, *28*, 31−43.

King, D. A. (1997). The functional significance of leaf angle in *Eucalyptus*. *Australian Journal of Botany*, *45*, 619−639.

Knyazikhin, Y., Martonchik, J. V., Myneni, R. B., Diner, D. J., & Running, S. W. (1998). Synergistic algorithm for estimating vegetation canopy leaf area index and fraction of absorbed photosynthetically active radiation from MODIS and MISR data. *Journal of Geophysical Research, [Atmospheres]*, *103*, 32257−32275.

Kubelka, P., & Munk, F. (1931). Ein Betrag zur Optik der Farbanstriche. *Zeitschrift für Technische Physik*, *12*, 593−601.

Laclau, J. P., Almeida, J. C. R., Goncalves, J. L. M., Saint-Andre, L., Ventura, M., Ranger, J., et al. (2009). Influence of nitrogen and potassium fertilization on leaf lifespan and allocation of above-ground growth in *Eucalyptus* plantations. *Tree Physiology*, *29*, 111−124.

Laclau, J. -P., Ranger, J., de Moraes Gonçalves, J. L., Maquère, V., Krusche, A. V., M'Bou, A. T., et al. (2010). Biogeochemical cycles of nutrients in tropical *Eucalyptus* plantations: Main features shown by intensive monitoring in Congo and Brazil. *Forest Ecology and Management*, *259*, 1771−1785.

Landsberg, J. J., & Waring, R. H. (1997). A generalised model of forest productivity using simplified concepts of radiation-use efficiency, carbon balance and partitioning. *Forest Ecology and Management*, *95*, 209−228.

le Maire, G., Francois, C., & Dufrene, E. (2004). Towards universal broad leaf chlorophyll indices using PROSPECT simulated database and hyperspectral reflectance measurements. *Remote Sensing of Environment*, *89*, 1−28.

le Maire, G., François, C., Soudani, K., Berveiller, D., Pontailler, J. -Y., Bréda, N., et al. (2008). Calibration and validation of hyperspectral indices for the estimation of broadleaved forest leaf chlorophyll content, leaf mass per area, leaf area index and leaf canopy biomass. *Remote Sensing of Environment*, *112*, 3846−3864.

le Maire, G., Francois, C., Soudani, K., Davi, H., Le Dantec, V., Saugier, B., et al. (2006). Forest leaf area index determination: A multiyear satellite-independent method based on within-stand normalized difference vegetation index spatial variability. *Journal of Geophysical Research*, *111*, G02027, doi:10.1029/2005JG000122.

le Maire, G., Marsden, C., Laclau, J. -P., Stape, J. -L., Corbeels, M., & Nouvellon, Y. (2010). Spatial and temporal variability of the carbon budget of tropical eucalyptus plantations assessed using ecosystem modelling and remote-sensing. *International conference on integrative landscape modelling (Landmod2010)* Montpellier: Edition Quae Symposcience. http://www.symposcience.fr/exl-doc/colloque/ART-00002412.pdf

Macfarlane, C., Arndt, S. K., Livesley, S. J., Edgar, A. C., White, D. A., Adams, M. A., et al. (2007). Estimation of leaf area index in eucalypt forest with vertical foliage, using cover and fullframe fisheye photography. *Forest Ecology and Management*, *242*, 756−763.

Marsden, C., le Maire, G., Stape, J. -L., Seen, D. L., Roupsard, O., Cabral, O., et al. (2010). Relating MODIS vegetation index time-series with structure, light absorption and stem production of fast-growing *Eucalyptus* plantations. *Forest Ecology and Management*, *259*, 1741−1753.

Medhurst, J. L., & Beadle, C. L. (2001). Crown structure and leaf area index development in thinned and unthinned *Eucalyptus nitens* plantations. *Tree Physiology*, *21*, 989−999.

North, P. R. J. (2002). Estimation of fAPAR, LAI, and vegetation fractional cover from ATSR-2 imagery. *Remote Sensing of Environment*, *80*, 114−121.

Nouvellon, Y., Laclau, J. -P., Epron, D., Kinana, A., Mabiala, A., Roupsard, O., et al. (2010). Within-stand and seasonal variations of specific leaf area in a clonal *Eucalyptus* plantation in the Republic of Congo. *Forest Ecology and Management*, *259*, 1796−1807.

Nouvellon, Y., Moran, M. S., Lo Seen, D., Bryant, R., Rambal, S., Ni, W. M., et al. (2001). Coupling a grassland ecosystem model with Landsat imagery for a 10-year simulation of carbon and water budgets. *Remote Sensing of Environment*, *78*, 131−149.

O'Grady, A. P., Worledge, D., Wilkinson, A., & Battaglia, M. (2008). Photosynthesis and respiration decline with light intensity in dominant and suppressed *Eucalyptus globulus* canopies. *Functional Plant Biology*, *35*, 439−447.

Pinkard, E. A., Patel, V., & Mohammed, C. (2006). Chlorophyll and nitrogen determination for plantation-grown *Eucalyptus nitens* and *E. globulus* using a non-destructive meter. *Forest Ecology and Management*, *223*, 211−217.

Ponzoni, F. J., & Goncalves, J. L. D. (1999). Spectral features associated with nitrogen, phosphorus, and potassium deficiencies in *Eucalyptus saligna* seedling leaves. *International Journal of Remote Sensing*, *20*, 2249−2264.

Press, W., Teukolsky, S., Vetterling, W., & Flannery, B. (1996). *Numerical recipes in Fortran 77* (second edition). New York: Cambridge University Press.

Privette, J. L., Myneni, R. B., Emery, W. J., & Pinty, B. (1995). Inversion of a soil bidirectional reflectance model for use with vegetation reflectance models. *Journal of Geophysical Research, [Atmospheres]*, *100*, 25497−25508.

Rouse, J. W., Haas, R. H., Schell, J. A., & Deering, D. W. (1973). Monitoring vegetation systems in the great plains with ERTS. In N. SP-351 (Ed.), *Third ERTS symposium* (pp. 309−317). Washington.

Saltelli, A., & Bolado, R. (1998). An alternative way to compute Fourier amplitude sensitivity test (FAST). *Computational Statistics and Data Analysis*, *26*, 445−460.

Saltelli, A., Tarantola, S., & Chan, K. P. -S. (1999). A quantitative model-independent method for global sensitivity analysis of model output. *Technometrics*, *41*, 39−56.

Sands, P. J., & Landsberg, J. J. (2002). Parameterisation of 3-PG for plantation grown *Eucalyptus globulus*. *Forest Ecology and Management*, *163*, 273−292.

SIMLAB (2009). Version 2.2, simulation environment for uncertainty and sensitivity analysis. *Developed by the Joint Research Centre of the European Commission* http://simlab.jrc.ec.europa.eu/

Soudani, K., Francois, C., le Maire, G., Le Dantec, V., & Dufrene, E. (2006). Comparative analysis of IKONOS, SPOT, and ETM+data for leaf area index estimation in temperate coniferous and deciduous forest stands. *Remote Sensing of Environment*, *102*, 161−175.

Soudani, K., le Maire, G., Dufrêne, E., François, C., Delpierre, N., Ulrich, E., et al. (2008). Evaluation of the onset of green-up in temperate deciduous broadleaf forests derived from Moderate Resolution Imaging Spectroradiometer (MODIS) data. *Remote Sensing of Environment*, *112*, 2643−2655.

Stape, J. L., Binkley, D., & Ryan, M. G. (2008). Production and carbon allocation in a clonal *Eucalyptus* plantation with water and nutrient manipulations. *Forest Ecology and Management*, *255*, 920−930.

Suits, G. H. (1972). The calculation of the directional reflectance of a vegetative canopy. *Remote Sensing of Environment*, *2*, 117−125.

Thenkabail, P. S., Smith, R. B., & De Pauw, E. (2000). Hyperspectral vegetation indices and their relationships with agricultural crop characteristics. *Remote Sensing of Environment*, *71*, 158−182.

Turner, D. P., Cohen, W. B., Kennedy, R. E., Fassnacht, K. S., & Briggs, J. M. (1999). Relationships between leaf area index and landsat TM spectral vegetation indices across three temperate zone sites. *Remote Sensing of Environment*, *70*, 52−68.

Utsugi, H., Araki, M., Kawasaki, T., & Ishizuka, M. (2006). Vertical distributions of leaf area and inclination angle, and their relationship in a 46-year-old *Chamaecyparis obtusa* stand. *Forest Ecology and Management*, *225*, 104−112.

Verhoef, W. (1984). Light scattering by leaf layers with application to canopy reflectance modeling: The SAIL model. *Remote Sensing of Environment*, *16*, 125−141.

Verhoef, W., & Bach, H. (2007). Coupled soil-leaf-canopy and atmosphere radiative transfer modeling to simulate hyperspectral multi-angular surface reflectance and TOA radiance data. *Remote Sensing of Environment*, *109*, 166−182.

Viovy, N., François, C., Bondeau, A., Krinner, G., Polcher, J., Kergoat, L., et al. (2001). Assimilation of remote sensing measurements into the ORCHIDEE/STOMATE DGVM biosphere model. *Recueil des actes du 8ème Symposium International "Mesures Physiques et Signatures en Télédétection"* (pp. 713−718). France: Aussois.

Walthall, C., Dulaney, W., Anderson, M., Norman, J., Fang, H., & Liang, S. (2004). A comparison of empirical and neural network approaches for estimating corn and soybean leaf area index from Landsat ETM+imagery. *Remote Sensing of Environment*, *92*, 465−474.

Weiss, M., & Baret, F. (1999). Evaluation of canopy biophysical variable retrieval performances from the accumulation of large swath satellite data. *Remote Sensing of Environment*, *70*, 293−306.

Wolfe, R. (2006). MODIS geolocation. *Earth Science Satellite Remote Sensing*, 50−73.

Xiao, Z. Q., Liang, S. L., Wang, J. D., Song, J. L., & Wu, X. Y. (2009). A temporally integrated inversion method for estimating leaf area index from MODIS data. *Geoscience and Remote Sensing, IEEE Transactions on*, *47*, 2536−2545.

Zurita-Milla, R., Kaiser, G., Clevers, J. G. P. W., Schneider, W., & Schaepman, M. E. (2009). Downscaling time series of MERIS full resolution data to monitor vegetation seasonal dynamics. *Remote Sensing of Environment*, *113*, 1874−1885.